Blade Loading and Its Application in the Mean-Line Design of Low Pressure Turbines

John D. Coull[1]
e-mail: jdc38@cam.ac.uk

Howard P. Hodson
e-mail: hph1000@cam.ac.uk

Whittle Laboratory,
University of Cambridge,
1 J.J. Thomson Ave,
Cambridge CB3 0DY, UK

*In order to minimize the number of iterations to a turbine design, reasonable choices of the key parameters must be made at the preliminary design stage. The choice of blade loading is of particular concern in the low pressure (LP) turbine of civil aero engines, where the use of high-lift blades is widespread. This paper considers how blade loading should be measured, compares the performance of various loss correlations, and explores the impact of blade lift on performance and lapse rates. To these ends, an analytical design study is presented for a repeating-stage, axial-flow LP turbine. It is demonstrated that the long-established Zweifel lift coefficient (Zweifel, 1945, "The Spacing of Turbomachine Blading, Especially with Large Angular Deflection" Brown Boveri Rev., **32**(1), pp. 436–444) is flawed because it does not account for the blade camber. As a result the Zweifel coefficient is only meaningful for a fixed set of flow angles and cannot be used as an absolute measure of blade loading. A lift coefficient based on circulation is instead proposed that accounts for the blade curvature and is independent of the flow angles. Various existing profile and secondary loss correlations are examined for their suitability to preliminary design. A largely qualitative comparison demonstrates that the loss correlations based on Ainley and Mathieson (Ainley and Mathieson, 1957, "A Method of Performance Estimation for Axial-Flow Turbines," ARC Reports and Memoranda No. 2974; Dunham and Came, 1970, "Improvements to the Ainley-Mathieson Method of Turbine Performance Prediction," Trans. ASME: J. Eng. Gas Turbines Power, July, pp. 252–256; Kacker and Okapuu, 1982, "A Mean Line Performance Method for Axial Flow Turbine Efficiency," J. Eng. Power, **104**, pp. 111–119). are not realistic, while the profile loss model of Coull and Hodson (Coull and Hodson, 2011, "Predicting the Profile Loss of High-Lift Low Pressure Turbines," J. Turbomach., **134**(2), pp. 021002) and the secondary loss model of (Traupel, W, 1977, Thermische Turbomaschinen, Springer-Verlag, Berlin) are arguably the most reasonable. A quantitative comparison with multistage rig data indicates that, together, these methods over-predict lapse rates by around 30%, highlighting the need for improved loss models and a better understanding of the multistage environment. By examining the influence of blade lift across the Smith efficiency chart, the analysis demonstrates that designs with higher flow turning will tend to be less sensitive to increases in blade loading.* [DOI: 10.1115/1.4006588]

1 Introduction

1.1 The Smith Efficiency Chart. Perhaps the most famous correlation for turbine efficiency is that proposed by Smith [1]. Using a large set of turbine test-rig data, he calculated the equivalent efficiency for each turbine with zero tip gap. Plotting the results against stage loading coefficient and flow coefficient, he obtained the efficiency chart shown in Fig. 1 for designs with 50% reaction. This plot shows that the efficiency tends to decrease as either the stage loading or the flow coefficient are increased. To illustrate the changes across the Smith chart design space, four diagrams indicating the approximate flow angles and possible blade shapes have been added.

As the flow coefficient is increased (moving from the bottom left to the bottom right of Fig. 1), the through-flow velocities increase relative to the blade speed as the flow becomes more axial. For a given change in tangential velocity, this causes an increase in the dynamic pressures which tends to increase the losses. Furthermore, losses increase because there is a smaller overall acceleration through the blade row. Such acceleration is beneficial as it tends to minimize the growth of the boundary layers and secondary flows.

As the stage loading coefficient is increased (moving from the bottom left to the top left of Fig. 1), the change in tangential velocity across the blade row becomes larger. To achieve this additional turning one must either employ blades with higher circulation (loading), or decrease the pitch (while maintaining circulation). Both changes tend to increase loss, as does the high exit flow angle from these designs (see Eq. (14) below).

1.2 Motivation and Scope of the Current Work. The Smith chart provides a simple guide for the selection of flow angles, but it does not capture the influence of other key parameters. Modern LP turbines typically feature high-lift blade designs, which can suffer a rapid drop in efficiency at the low Reynolds number conditions experienced at cruise [8]. Ultimately, it is highly desirable to accurately capture these effects at the earliest stages of design.

The simplest model for turbomachine design is mean-line modeling, where the flow is represented by the mean flow quantities at each inter-blade gap. Due to its simplicity, this analysis is well suited to understanding trends across the design space, but it must rely on empirical correlations for profile, secondary and tip leakage losses. Notable examples of loss correlations include those of Craig and Cox [9], Traupel [7] and Ainley and Mathieson [3], which was later updated by Dunham and Came [4] and Kacker and Okapuu [5]. While these models take account of blade loading, none are influenced by the shape of the blade surface pressure distributions, which can have a strong influence on LP turbine performance (e.g., Refs. [10,11]). A profile loss model was recently

[1]Corresponding author.

Contributed by the International Gas Turbine Institute (IGTI) of ASME for publication in the JOURNAL OF TURBOMACHINERY. Manuscript received August 24, 2011; final manuscript received October 6, 2011; published online November 8, 2012. Editor: David Wisler.

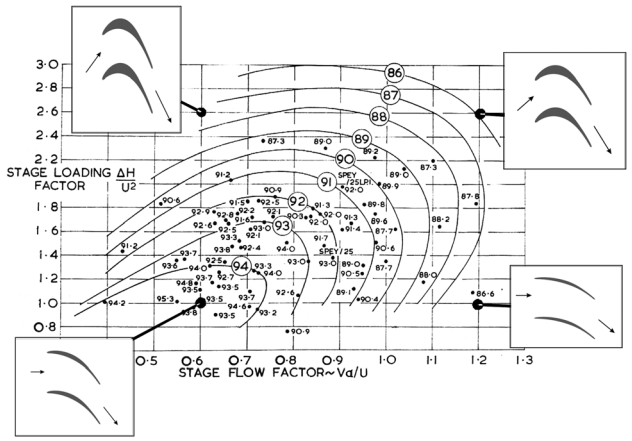

Fig. 1 Turbine stage efficiency normalized for zero tip gap, 50% reaction designs, Smith [8]

developed for high-lift LP turbine blades by the current authors to capture such effects [6].

This paper outlines a mean-line design study for a repeating-stage LP turbine, making use of published loss correlations. The analytical methods are described in Sec. 3. Section 4 examines how blade loading should be quantified and demonstrates that the standard Zweifel lift coefficient [2] is unsuitable for this purpose. Section 5 evaluates various profile and secondary loss correlations. This analysis first concentrates on the qualitative trends predicted for varying flow angles, loading and Reynolds number before a quantitative comparison of lapse rates is performed. Finally, Sec. 6 examines the sensitivity of the Smith efficiency chart to increases in blade loading.

3 Analytical Methods for Design Study

3.1 Datum Turbine. In order to provide a reference for the subsequent analysis, a datum turbine design is considered that is approximately representative of modern LP turbine designs. The details of the design are presented in Table 1. The datum turbine is a repeating stage with 50% reaction. The flow coefficient (0.9) and stage loading (2) place the datum design approximately in the middle of the Smith chart design space (Fig. 1). The Reynolds numbers are roughly representative of modern LP turbines at cruise conditions. The reduced frequency f_r describes the frequency of wakes arriving from the upstream blade row, which can be accounted for in the profile loss model of Ref. [5]. The influence of this parameter is largely second-order, and will not be discussed further in this paper, though its effect has been included in the analysis. The specified blade aspect ratios are based on the axial chord, since the designer will be interested in the overall stage length. The chosen aspect ratios set the ratio of stator to rotor blades at approximately 1:1.4. The stage has a constant mean radius and the area ratio through the stage expands to maintain constant axial velocity though the stage. The tip gap is assumed to be zero throughout this analysis, which allows direct comparison with the efficiencies on the Smith chart. For simplicity, the analysis here has been performed at relatively low speed and the Mach number is not included in Table 1 since it has only a weak influence on performance. While analysis at higher speeds shows that Mach number variations do have an influence on efficiency, this does not affect the conclusions that can be drawn from the analysis.

3.2 A Study of Comparable Designs. The current design study has been conducted with the industrial design process in mind. The multistage LP turbine has three key overall requirements which are set by the engine architecture: the core mass flow rate is determined by the engine bypass ratio, while the required power output and shaft speed are fixed by the requirements of the fan. The designer must choose the number of stages for the LP turbine, which sets the power output per stage. When comparing different turbine designs, one must therefore consider designs with the same stage power output, mass flow rate and shaft RPM as the datum case, for the same inlet conditions. As shall be demonstrated, this requirement results in turbines of different mean radius and flow area as the flow angles are varied.

Table 1 Design and flow parameters for the datum repeating-stage turbine; "*" indicates a parameter that remains constant in the subsequent design space study

Flow Angles	
Reaction (Λ)	50%*
Flow Coefficient (ϕ)	0.9
Stage Loading Coefficient (ψ)	2
Repeating Stages Assumed*	
Non-dimensional flow parameters	
Stator Reynolds number (Re_{S_0})	250,000
Equivalent Re_C	194,000
Rotor Reynolds number (Re_{S_0})	177,000
Equivalent Re_C	138,000
Stator reduced frequency (f_r)	1.31
Rotor reduced frequency (f_r)	0.67
Geometric Parameters	
Hub-to-tip ratio (average for stage)	0.75
Rotor Aspect Ratio (h/C_x)	6.50*
Stator Aspect Ratio (h/C_x)	4.60*
Trailing edge thickness (t_{TE}/C)	0.01*
Zero Tip gap	0*
Mean radius constant through the stage*	
V_x constant through the stage*	
Blade Velocity Distributions	
Circulation Coefficient (Equation (21))	0.70
Peak Velocity Location (fraction of S_0)	45%*
Leading Edge Integral	50%*
Diffusion Factor (DF)	0.21

3.3 Flow Parameters and Gas Angles. Figure 2 shows a schematic of the two-dimensional flow through a turbine stage for constant axial velocity. It also defines the sign conventions for the flow angles.

In this study the stage reaction is fixed at 0.5 (Table 1), so:

$$\alpha_1 = -\beta_2, \quad \alpha_2 = -\beta_3 \tag{1}$$

The stage is repeating, so that:

$$\alpha_3 = \alpha_1 \tag{2}$$

The gas angles are therefore fixed by the choice of Flow Coefficient ϕ and Stage Loading Coefficient ψ:

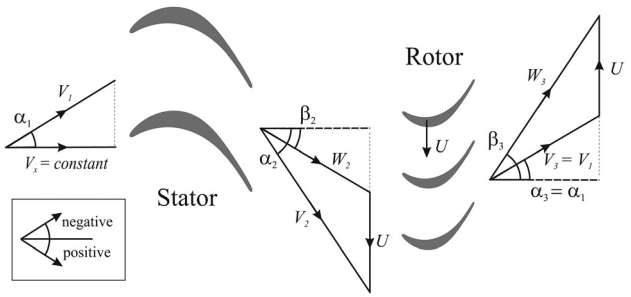

Fig. 2 Velocity triangles and angle conventions

$$\psi = 2\,(0.5 - \phi\,\tan\alpha_1) \tag{3}$$

$$\psi = \phi\,(\tan\alpha_2 - \tan\alpha_1) \tag{4}$$

3.4 Calculation Procedure. For a fixed stage power output $\dot{w}_x$ and mass flow rate $\dot{m}$, the blade speed U is set by the stage loading coefficient:

$$U = \sqrt{\frac{\dot{w}_x}{\dot{m}\,\psi}} \tag{5}$$

Noting that one is considering designs for a fixed rotational shaft speed, the mean radius is thus given by:

$$r_{\text{mean}} = \frac{U}{\omega_s} = \frac{1}{\omega_s}\sqrt{\frac{\dot{w}_x}{\dot{m}\,\psi}} \tag{6}$$

The flow coefficient sets the axial velocity:

$$V_x = \phi\,U = \phi\sqrt{\frac{\dot{w}_x}{\dot{m}\,\psi}} \tag{7}$$

Together with the flow angles, the inter-blade velocities can now be calculated:

$$V_i = V_x/\cos\alpha_i \tag{8}$$

$$W_i = V_x/\cos\beta_i \tag{9}$$

where the index i represents each inter-blade gap (Fig. 2). Figure 3(*a*) shows the variation of the exit velocity from the stator row (normalized by the datum value), which is largest for designs with high flow coefficient and low stage loading.

Compressible flow relationships are then used to determine the Mach numbers, and hence the total and static values of pressure, temperature and density at the inlet and exit of each blade row. To correctly calculate the total pressures throughout the stage, the loss coefficients must be known: the calculation is therefore iterated to arrive at the correct result.

Together with the specified mass flow rate, the calculated density determines the flow area, which expands through the machine to maintain constant axial velocity. The flow area determines the span: Fig. 3(*b*) shows the variation over the design space. The span is largest for designs with high stage loading and low flow coefficients, which have low axial velocity. Together with the specified aspect ratios (Table 1), the axial chords of the stators and rotors are thus determined.

It is necessary at this point to make some estimates of the blade geometry, since some loss correlations rely on true chord, camber-line length and surface lengths. The relationships between these geometric parameters will be very different for high and low

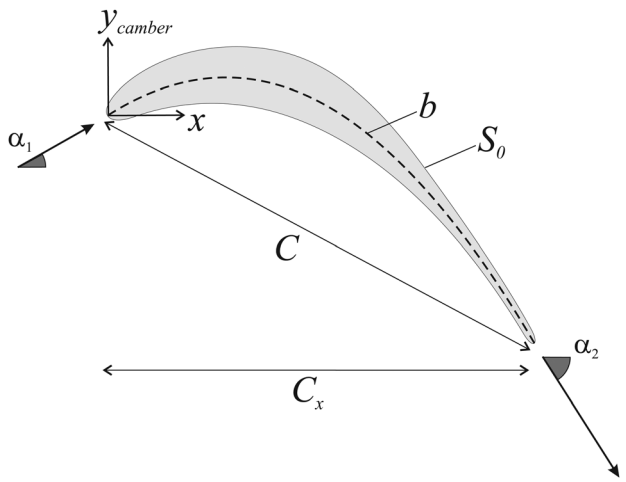

Fig. 4 Geometry estimation using a parabolic camberline

turning airfoils. It is first assumed that the camber-line of a blade can be approximated by a parabolic curve, which was shown to be reasonable by Horlock [12]:

$$y_{\text{camber}} = A\,x^2 + B\,x \tag{10}$$

The basic approach is illustrated in Fig. 4. The camber-line of the blade is assumed to align with the flow angles at inlet and exit, uniquely setting the constants A and B in Eq. (10). The length of the camber-line b and the true chord C may then be calculated from the known axial chord C_x. The length of the blade suction surface S_0 will largely depend on the camber-line of the blade, and so the following simple relationship was proposed:

$$S_0 = 1.15\,b \tag{11}$$

The factor of 1.15 is based on a survey of LP turbine blades from the literature. Figure 3(*c*) shows the ratio of this estimated surface length to the axial chord over the design space. In reality the thickness distribution of the turbine blade will also make a contribution to the surface length, but Eq. (11) is sufficiently accurate for the current purposes.

For profile losses, the appropriate Reynolds number is based on the suction surface length and exit velocity ([5]). Figure 3(*d*) demonstrates that this parameter is large for highly turning designs; the variation in suction surface length (Fig. 3(*c*)) therefore dominates the variation in exit flow velocity (Fig. 3(*b*)) in setting the Reynolds number.

3.5 Surface Velocity Distributions, Pitch and Loss Prediction. One of the profile loss models considered in this paper is based on the preliminary design correlation previously

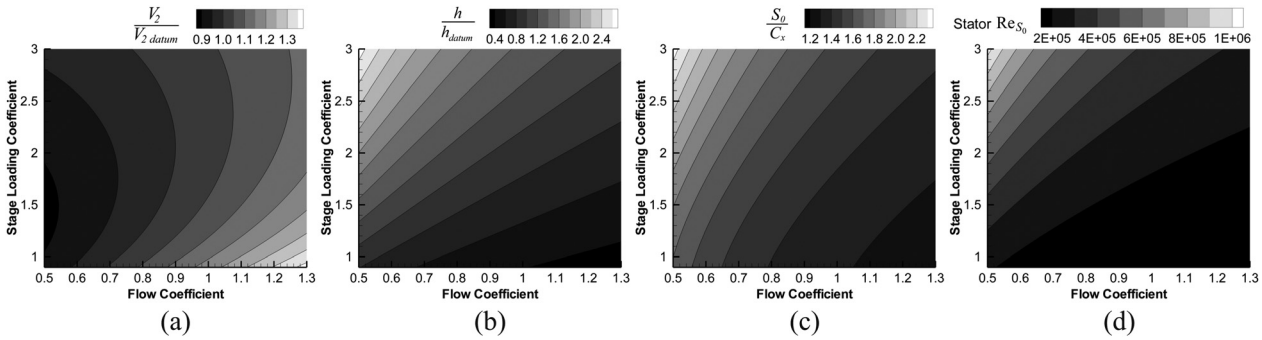

Fig. 3 Calculated flow and geometry parameters across the design space: (*a*) stator exit velocity; (*b*) mean span; (*c*) ratio of S_0/C_x; (*d*) Reynolds number

developed by the authors for high-lift blades featuring laminar separation bubbles [6]. This method relies on an empirical correlation for the boundary layer parameters at the suction surface trailing edge, based on the freestream velocity distribution over the surface. Effectively, a Thwaites [16] calculation (or equivalent) is performed up to the point of laminar separation; a correlation then relates the growth in momentum thickness through the separation bubble and downstream turbulent boundary layer. A separate correlation predicts the shape factor and hence the trailing edge displacement thickness.

Coull and Hodson [6] showed that, with certain assumptions, the suction surface velocity distribution can be modeled by three key design parameters: the diffusion factor, the peak velocity location on the surface and the leading edge integral, which describes the loading up to the velocity peak and is defined in Eq. (12).

$$\text{Leading Edge Integral} = LEI = \int_0^1 \left(\frac{V_s}{V_{\text{speak}}}\right)^5 d\left(\frac{S}{S_{\text{peak}}}\right) \tag{12}$$

Comparison with the method of Thwaites [16] demonstrates that this parameter is proportional to the square of the momentum thickness at the peak velocity location [6]. In this study the peak velocity was fixed at 45% of the surface, which is relatively far forwards on the surface. Front-loading in this manner reduces the deceleration rate over the rear portion of the blade and minimizes the losses generated by the separation bubble. The leading edge integral was fixed at 50%, which should be low enough to provide reasonable incidence tolerance. The diffusion factor was varied to achieve the required blade loading. Sample velocity distributions of the style assumed are shown in Fig. 5.

The blade pitch is related to the gas turning and the blade circulation, e.g., for the stator:

$$\frac{s}{S_o} = \frac{\oint \left(\frac{V_s}{V_2}\right) d\left(\frac{S}{S_0}\right)}{(\tan\alpha_1 - \tan\alpha_2)\cos\alpha_2} \tag{13}$$

The profile loss may be related to the predicted trailing edge boundary layer parameters using an approximation to the analytical solution of Denton [13]:

$$Y_p \approx \left(\frac{2\sum\theta_{TE}}{s\cos\alpha_2}\right) + \left(\frac{\sum\delta^*_{TE} + t_{TE}}{s\cos\alpha_2}\right)^2 \tag{14}$$

In Coull and Hodson [6], a correction was applied to Eqs. (13) and (14) to account for the depression of the freestream velocity in the vicinity of the trailing edge. This correction has not been used in the current study because there is insufficient data to predict this velocity depression for low or high turning designs. Instead, it has been assumed that the freestream velocity at the trailing edge is equal to the mean exit flow velocity from the blade row. This assumption will have only a minor impact on the results of this study.

In addition to the Coull and Hodson method, this paper considers several other profile loss models ([3–5,9,13]), and secondary loss models ([3–5,7,9,17]).

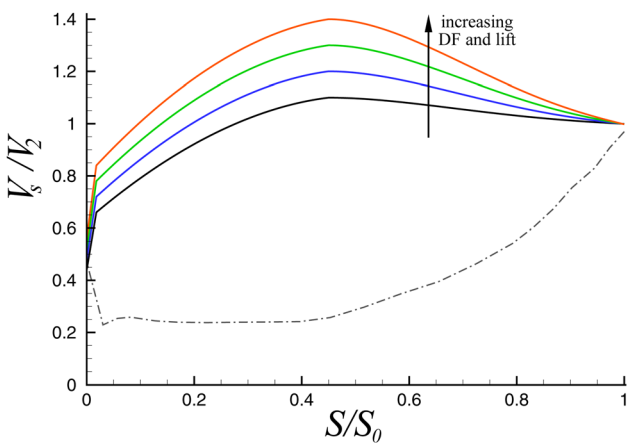

Fig. 5 Sample surface velocity distributions

3.6 Relating Loss Coefficients to Stage Efficiency. It should be noted that most of the loss correlations are based on total pressure loss coefficients obtained at low Mach numbers. Such total pressure losses tend to have a relatively strong Mach number dependence, and this effect would therefore need to be accounted for in the analysis. Fortunately this issue can be largely avoided by using the energy loss coefficient, defined for the stator row as:

$$\varsigma = \frac{V_{2,is}^2 - V_2^2}{V_{2,is}^2} \equiv Y \text{ for incompressible flow} \tag{15}$$

where $V_{2,is}$ is the exit velocity obtained by isentropic expansion from the inlet total pressure to the exit static pressure. The energy loss coefficient has a much lower dependency on Mach number than the total pressure loss coefficient, and may therefore be reliably used for flows with a peak Mach numbers below around 0.85 ([18,19]). This is an approximation, but it is sufficiently accurate for this study.

The total-total isentropic efficiency for the repeating stage is defined as:

$$\eta = \frac{h_{01} - h_{02}}{h_{01} - h_{02,is}} = \frac{T_{01} - T_{02}}{T_{01} - T_{02,is}} \tag{16}$$

4 Lift Coefficients

4.1 Zweifel Lift Coefficient. The Zweifel lift coefficient [2] is a widely-used measure of blade loading. It is defined as the ratio of the tangential force on a blade to an "ideal" case, where the flow on the pressure surface of the blade is stagnated ($P = P_0$), while the flow over the suction surface travels at the mean exit velocity from the blade row ($P = P_2$). The Zweifel coefficient is therefore given by:

$$Z_w = \frac{\oint P\,\mathrm{d}x}{C_x(P_{01} - P_2)} \tag{17}$$

From a control volume analysis, the tangential force can be related to the flow angles, giving:

$$Z_w = \frac{\dot{m}_{\text{passage}}\,\Delta V_\theta}{hC_x(P_{01} - P_2)} \tag{18}$$

These equations can be simplified for the case of incompressible flow. From Eq. (17), the Zweifel coefficient can be calculated by integrating the square of the freestream velocity over the blade surfaces:

$$Z_w = \frac{\oint 0.5\,\rho\,V_s^2 dx}{C_x\,0.5\,\rho\,V_2^2} = \oint (V_s/V_2)^2\, d(x/C_x) \tag{19}$$

This definition is illustrated graphically in Fig. 6(*a*). For low Mach numbers and constant axial velocity, Eq. (18) may be rewritten as:

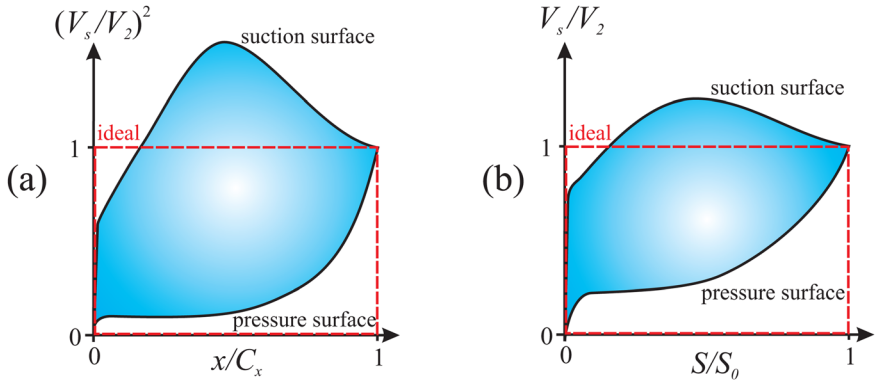

Fig. 6 Low speed definition of: (*a*) Zweifel lift coefficient Z_w (Eq. (19)); (*b*) Circulation coefficient C_o (Eq. (21))

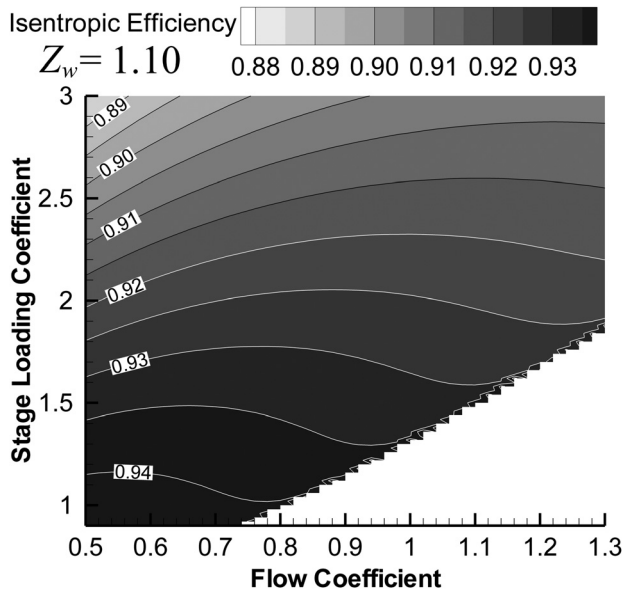

Fig. 7 Predicted efficiency for constant $Z_w = 1.10$ using the models of Refs. [6] and [7]

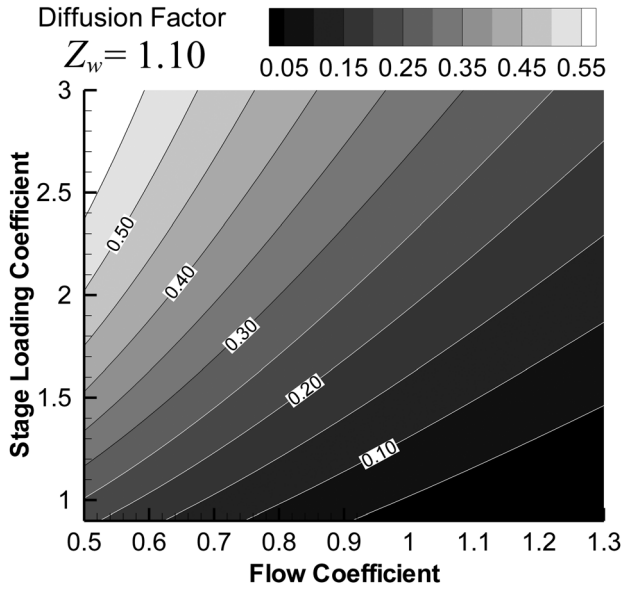

Fig. 8 Diffusion factor for constant $Z_w = 1.10$ using the models of Refs. [6] and [7]

$$Z_w = \frac{\dot{m}_{\text{passage}}\,\Delta V_\theta}{C_x\,0.5\,\rho\,V_2^2} = \frac{s}{C_x}\left(\frac{\tan\alpha_2 - \tan\alpha_1}{0.5\sec^2\alpha_2}\right) \tag{20}$$

Mean-line efficiency predictions have been performed for a constant value of Zweifel coefficient ($Z_w = 1.1$) and are presented in Fig. 7. The profile and secondary loss models used are those of Coull and Hodson [6] and Craig and Cox [9], respectively. (The justification for using these methods is presented in the following section.) There are some similarities to Smith's efficiency chart (Fig. 1), in particular the decrease of efficiency with increased stage loading. However, the decrease of efficiency with increasing flow coefficient (towards the right of Fig. 1) has not been captured. There is also a region in the bottom right without data, the reason for which will be made clear in the following plot. For constant a Zweifel coefficient, the trends in the Smith chart could not be satisfactorily reproduced using any of the loss correlations considered in this paper.

Figure 8 shows the variation in diffusion factor (*DF*) across the Smith-chart design space; this parameter varies to maintain a constant Zweifel coefficient as the flow angles change. The plot shows that the diffusion factor varies significantly across the design space. The maximum value of around 0.6 occurs for the designs with the highest turning (low ϕ, high ψ), which are likely to undergo turbulent separation. At the other end of the design space, the diffusion factor is only around 0.05, and these designs will therefore tend to exhibit attached laminar flow over the full length of the suction surface. (The reason for the blanked region in Fig. 7 is that the profile loss model is not valid for permanently attached flow.) Therefore, the same Zweifel coefficient simultaneously describes very highly loaded blades suffering turbulent separation, very lightly loaded blades with laminar attached flow, and everything in-between. The Zweifel coefficient is therefore an inappropriate parameter to compare designs with different flow angles.

4.2 Circulation Coefficient. A new lift coefficient based on the blade circulation is proposed. In a manner analogous to the Zweifel coefficient, the *Circulation Coefficient* C_o is defined as the ratio of the blade circulation to an ideal circulation, with $V_s = V_2$ on the suction surface and stagnated flow ($V_s = 0$) on the pressure surface:

$$C_o = \frac{\text{actual circulation}}{\text{ideal circulation}} = \frac{\oint V_s\,\mathrm{d}S}{V_2\,S_0} = \oint\left(\frac{V_s}{V_2}\right)d\left(\frac{S}{S_0}\right) \tag{21}$$

This low-speed definition is illustrated graphically in Fig. 6(*b*). A suitable scaling for compressible flow must also be considered.

Several authors (e.g., Refs. [18] and [19]) have demonstrated that, for peak Mach numbers less than around 0.85, a given high-speed blade will have the same performance as a low-speed blade with the same exit angle and a matching surface distribution of the pressure coefficient:

$$C_p = \frac{P_{01} - P}{P_{01} - P_2} \tag{22}$$

Since the high-speed blade and its low-speed equivalent have the same performance, they must have the same circulation coefficient. For the equivalent low-speed blade, one notes that:

$$C_p = \frac{P_{01} - P}{P_{01} - P_2} = \left(\frac{V_s}{V_2}\right)^2 \tag{23}$$

The equivalent low-speed blade therefore has a circulation coefficient:

$$C_o = \oint \sqrt{\frac{P_{01} - P}{P_{01} - P_2}}\, d\left(\frac{S}{S_0}\right) = \oint \sqrt{C_p}\, d\left(\frac{S}{S_0}\right) \tag{24}$$

The distribution of C_p is identical for the high-speed blade and its low-speed equivalent, so this definition is appropriate for high-speed blades.

At low Mach numbers and constant V_x the circulation may be related to the flow angles and pitch (Eq. (13)) to give:

$$C_o = \frac{s}{S_0}\left(\frac{\tan\alpha_1 - \tan\alpha_2}{\sec\alpha_2}\right) \tag{25}$$

There are clear similarities between the circulation and Zweifel coefficients. Comparing Eqs. (20) and (25), the two coefficients are related by the following parameter:

$$\frac{C_o}{Z_W} = \left(\frac{0.5\, C_x}{S_0 \cos\alpha_2}\right) \tag{26}$$

This parameter varies depending on the camber of the blade. Therefore the fundamental difference between the circulation coefficient and Zweifel number is that the former takes into account the camber of the blade, while the latter does not. For a turbine comprised of inclined flat plates (i.e., no camber) the expression in Eq. (26) takes a value of 0.5; for extremely cambered blades it may be as high as 0.8. Equation (26) therefore implies that the circulation coefficient will always be lower than the Zweifel coefficient. This may at first seem odd since they are both defined relative to an ideal case; however Fig. 6 demonstrates graphically that the integration of V_s^2 in the Zweifel coefficient will be larger than the integration of V_s in the circulation coefficient.

Mean-line predictions were performed for designs with constant circulation coefficient. With a fixed pressure side velocity distribution, peak velocity location and leading edge loading, C_o uniquely sets the diffusion factor (Fig. 5). Thus a constant circulation coefficient implies constant surface velocity distributions over the Smith chart design space. Figure 9 shows the predicted efficiencies for $C_o = 0.70$ (implying $DF = 0.21$), again using the profile and secondary loss models of Coull and Hodson [5] and Craig and Cox [9], respectively. Remarkably good agreement with the trends of the original Smith chart in Fig. 1 is achieved. This result supports the use of the circulation coefficient rather than Zweifel. In many ways this conclusion is unsurprising: blade design typically focuses on the shape of the surface velocity or Mach number distributions, rather than the Zweifel coefficient.

5 Assessment of Loss Correlations

This section examines several profile and secondary loss correlations from the literature. Although the accuracy of each model cannot be directly evaluated without a large experimental dataset, any successful model should *at the very least* be able to predict the correct trends across the design space. The following subsections examine the influence of flow angles on profile and secondary losses respectively. This analysis is performed for the case shown in Fig. 9, with a constant circulation coefficient of $C_o = 0.70$. The sensitivity of the various models to blade loading and Reynolds number are then examined. Finally a quantitative comparison between predicted and measured lapse rates of multistage turbines is performed to examine absolute accuracy.

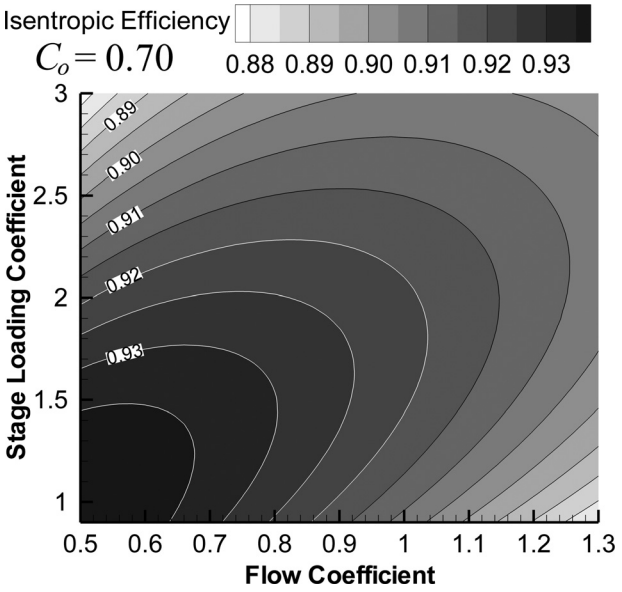

Fig. 9 Predicted stage efficiency for constant circulation coefficient $C_o = 0.70$ using the models of Refs. [6] and [7]

5.1 The Influence of Flow Angles - Profile Loss Models. While the overall trend of the Smith chart is well established, the contribution of profile and secondary losses is not immediately obvious. However, Denton [13] employed a simple analytical approach to examine the trends in profile loss across the Smith chart design space. From entropy considerations, the profile loss coefficient may be calculated by integrating V_s^3 over the blade surfaces:

$$\zeta_p \approx 2 \sum_{ss+ps} \frac{S_0}{s \cos\alpha_2} \int_0^1 C_d (V_s/V_2)^3 d(S/S_0) \tag{27}$$

The dissipation coefficient C_d will vary over the surface, depending on the boundary layer development and the Reynolds number. However an approximate prediction may be made by assuming that it takes a constant value typical of fully turbulent flow, $C_d = 0.002$. (For the fixed velocity distributions in the current analysis, this assumption effectively excludes Reynolds number influences.) The result in Fig. 10(*a*) shows that the lost efficiency increases as the flow turning increases, reaching a maximum in the top left of the Smith chart. This trend may be largely understood from Eq. (27). The loss coefficient rises strongly towards the top left of the Smith chart, where the exit flow angle α_2 increases and the ratio of pitch to suction surface length s/S_0 decreases (in order to perform more flow turning with constant circulation).

The profile lost efficiency predicted using the method of Coull and Hodson [5] is presented in Fig. 10(*b*). As for the Denton method, the losses increase as the flow turning increases, reaching a maximum in the top left of the Smith chart. The predicted loss is higher than the Denton predictions, which is unsurprising given that the dissipation coefficient will tend to be higher for laminar,

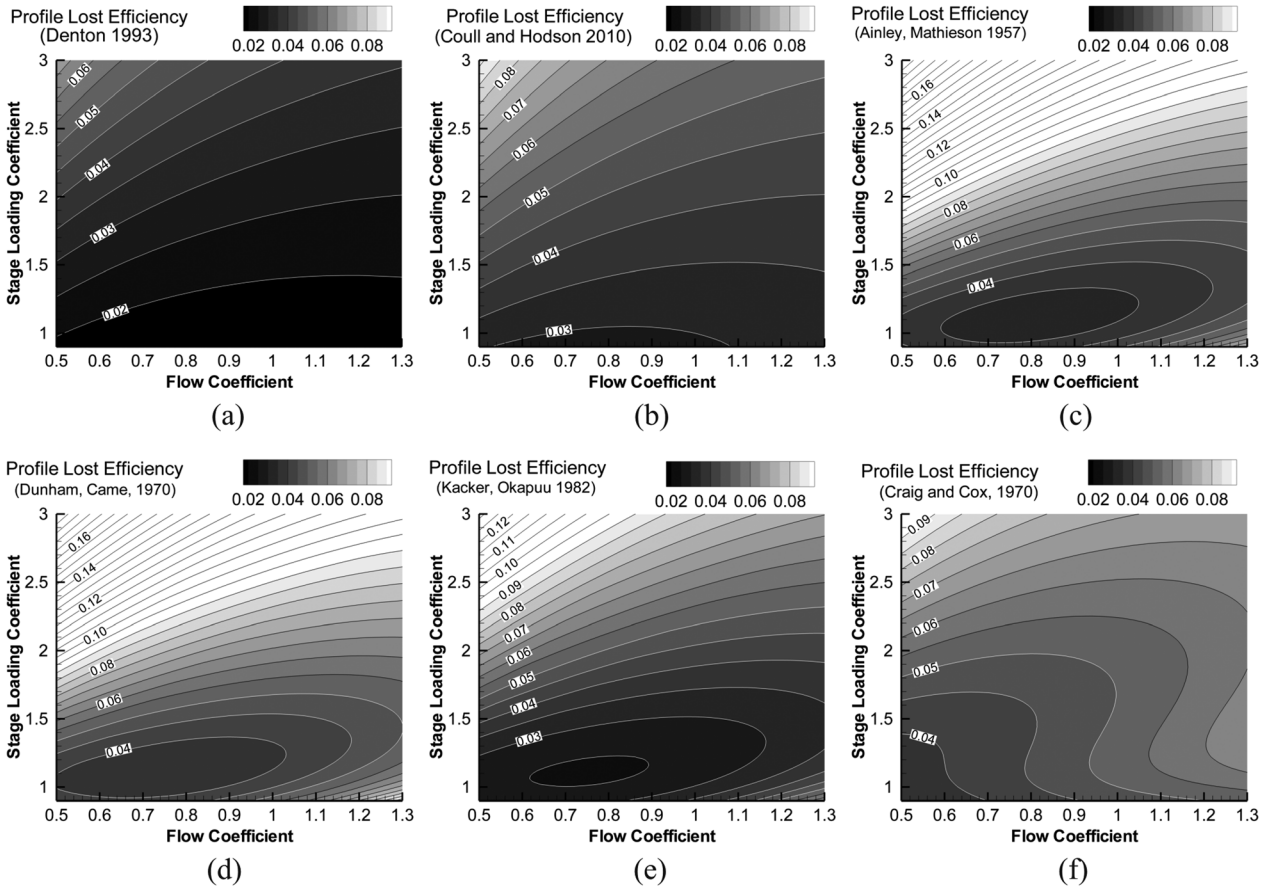

Fig. 10 Predicted lost efficiency due to profile loss for $C_o = 0.70$: (*a*) Denton [13]; (*b*) Coull and Hodson [6]; (*c*) Ainley and Mathieson [3]; (*d*) Dunham and Came [4]; (*e*) Kacker and Okapuu [5]; (*f*) Craig and Cox [7]

separated and transitional flows [13]. Figure 10(*b*) also shows a weak tendency for loss to increase at high flow coefficients, which is evident as a slight curling of the contours in the bottom right of the chart. This effect is driven by variations in Reynolds number (Fig. 3(*d*)) and exit dynamic pressure (from Fig. 3(*a*))[2].

Figure 10(*c*) shows the profile lost efficiency predicted by the method of Ainley and Mathieson [2], who interpolated between loss charts for "nozzle" blades with axial inlet flow (i.e., $\alpha_1 = 0$ for a stator), and impulse blades ($\alpha_1 = -\alpha_2$) for different flow angles and pitch-to-chord ratios. A correction is then made for the trailing edge thickness. The overall trend of Fig. 10(*c*) is somewhat similar to Fig. 10(*a*) and 10(*b*) except that high losses are predicted for low turning designs (high ϕ and low ψ), which is caused by extrapolating the method to the high pitch-to-chord ratios of these designs.[3] The predicted profile losses for designs with high turning (low ϕ and high ψ) are very high. In fact, even if the secondary losses are zero, this model predicts lower efficiency than was observed by Smith for such designs (Fig. 1).

Figure 10(*d*) and 10(*e*) show two later modifications of the Ainley and Mathieson method. Dunham and Came [3] accounted for Reynolds number and Mach number variations, which makes only small changes to the predictions (Fig. 10(*d*)). This model therefore suffers from the same problems as the original method. Kacker and Okapuu [4] suggested multiplying the Dunham and Came predictions by 2/3 (Fig. 10(*e*)), which produces more reasonable levels of efficiency. However the increase in losses for high-turning designs (high ψ and low ϕ) and low-turning designs (low ψ and high ϕ) is far more rapid than either the Coull and Hodson or the simple Denton methods suggest, and therefore does not appear to be realistic.

The profile lost efficiency predicted using the correlations of Craig and Cox [9] is presented in Fig. 10(*f*). Although the loss increases for high-turning designs, it also increases strongly as the flow coefficient rises, which does not match the simple Denton analysis in Fig. 10(*a*). (The kink in the data is due to extrapolation errors from Craig and Cox's charts.)

This comparison shows that the model of Coull and Hodson [5] gives the most realistic predictions of profile loss across the design space. This method also has higher fidelity than the others, since it depends on the shape of the blade velocity distributions rather than just the pitch.

5.2 The Influence of Flow Angles - Secondary Loss Models. Figure 11(*a*) shows the predicted lost efficiency due to the secondary loss model of Craig and Cox [9]. This plot shows that secondary losses are largely responsible for the observed drop in efficiency at high flow coefficients. Together with the increase in profile loss with the stage loading coefficient (Fig. 10(*b*)), the overall trend of the Smith chart is reproduced (Fig. 9). The variation across the design space in Fig. 11(*a*) is due to a combination of competing effects. The Craig and Cox correlations are presented graphically rather than as analytical expressions, but the trends of Fig. 11(*a*) are driven by variation in the following parameters, in approximately decreasing order of influence:

(1) Velocity ratio through the blade row. Secondary losses tend to be higher when there is a low overall acceleration through the stage. Designs with high flow coefficient and low stage loading therefore have high secondary losses.

[2]For a high speed datum turbine, this effect is slightly magnified due to the high Mach numbers in this region of the Smith chart.

[3]Note that these designs have low flow turning, so for a constant circulation they must have a high pitch-to-chord ratio.

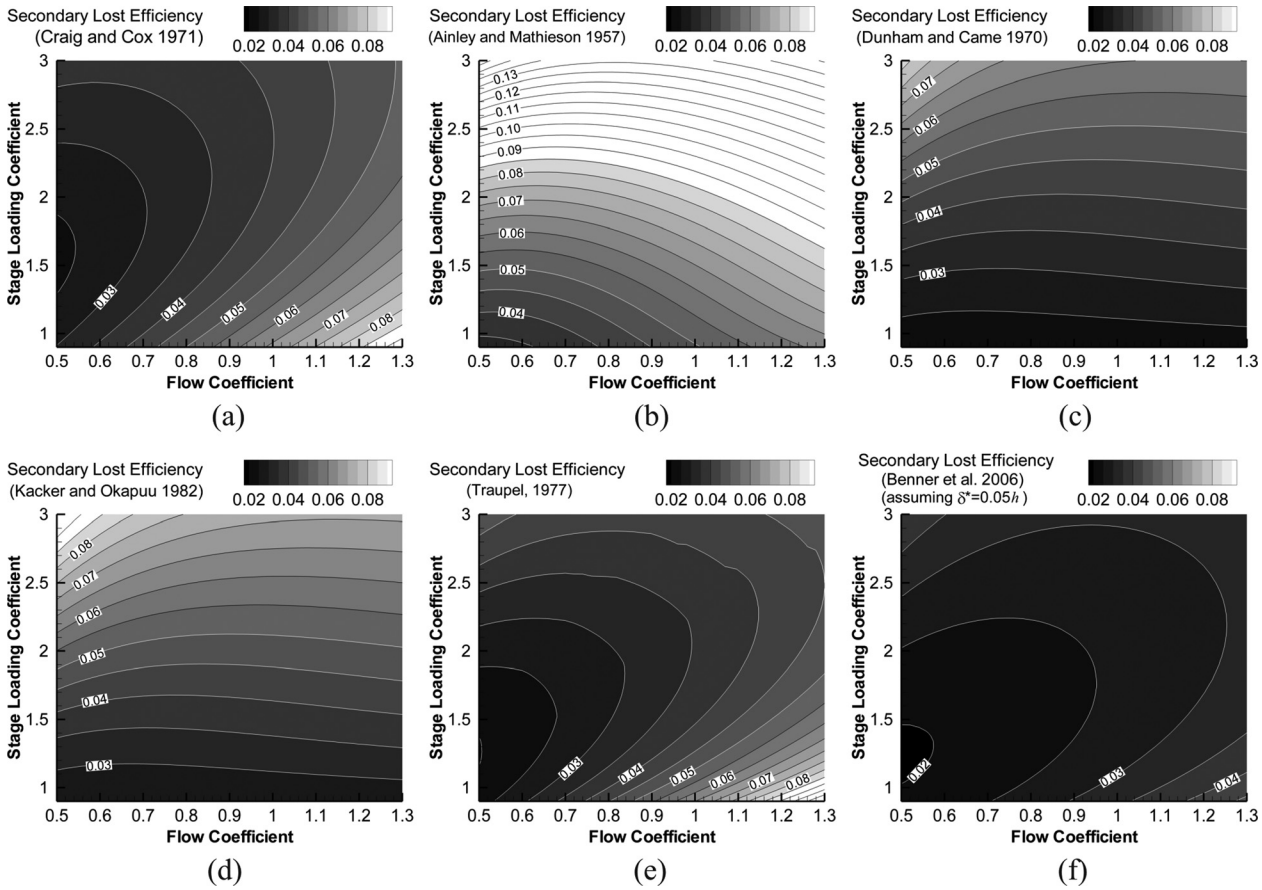

Fig. 11 Predicted lost efficiency due to secondary loss for $C_o = 0.70$, according to: (*a*) Craig and Cox [6]; (*b*) Ainley and Mathieson [3]; (*c*) Dunham and Came [4]; (*d*) Kacker and Okapuu [5]; (*e*) Traupel [7]; (*f*) Benner et al. [17]

(2) Exit dynamic pressure. Pressure losses scale with the dynamic pressure, which is high for designs with high flow coefficient and low stage loading (see Fig. 3(*b*)).
(3) Aspect ratio. Secondary losses increase as the aspect ratio is decreased. A constant aspect ratio h/C_x has been specified in this study, but the Craig and Cox correlation is sensitive to the ratio of span to camberline h/b, which decreases for highly cambered blades, driving a slight increase in secondary losses towards the top left of the Smith chart.
(4) Blade pitch. Increasing the blade pitch causes the secondary flow structures to develop to a larger size (since they are less restricted by the blade surfaces) and penetrate further towards the midspan region. Craig and Cox use the pitch-to-camberline ratio, which tends to be larger for designs with low stage loading coefficient.
(5) Lift coefficient. Highly loaded blades exhibit a stronger pressure difference between the suction and pressure surfaces; this pressure difference drives the overturning of the endwall flow. According to the Craig and Cox definition, designs with a higher stage loading coefficient have higher lift coefficients, and so tend to have higher secondary losses.
(6) Reynolds number. The Craig and Cox model assumes modest changes in secondary loss with Reynolds number, approximately following a turbulent trend ($\sim \mathrm{Re}^{-0.2}$).

The predicted secondary lost efficiency using the method of Ainley and Mathieson [3] is presented in Fig. 11(*b*). The observed trend is very different to the Craig and Cox result, and very high losses are predicted for designs with high stage loading coefficient. One is left wondering why the two methods give such different trends, and which is more representative of reality.

The details of the Ainley and Mathieson secondary loss model are given in Ref. [14]. They chose the following form for the secondary loss coefficient, based on the work of Carter [15]:

$$Y_s = \lambda \left(\frac{C_L}{s/C}\right)^2 \left(\frac{\cos^2 \alpha_2}{\cos^3 \alpha_m}\right) \tag{28}$$

where λ is a function of the effective inter-row flow areas and the hub-to-tip ratio. The vector-mean flow direction α_m is defined as:

$$\alpha_m = \tan^{-1}(\tan \alpha_1 + \tan \alpha_2) \tag{29}$$

The lift coefficient C_L is analogous to that for an external wing section, and is defined using the vector-mean velocity:

$$C_L = 2\left(\frac{s}{C}\right)(\tan \alpha_1 - \tan \alpha_2)\cos \alpha_m \tag{30}$$

The square of the lift coefficient in Eq. (28) drives the large increases in secondary loss at low flow coefficient and high stage loading (Fig. 11(*b*)). A similar effect was noted in point [5] above for the Craig and Cox method, but here the influence of lift coefficient dominates over the other effects.[4]

One problem with the Ainley and Mathieson method is that the definition of lift coefficient C_L (Eq. (30)) is not appropriate for moderate or highly cambered blades, as they themselves pointed out in Ref. [14]. For example, the vector-mean velocity for a high-turning impulse blade ($\alpha_1 = -\alpha_2$) is simply the axial velocity V_x, which is much smaller than the actual flow velocities in the cascade.

[4]It should be noted that Ainley and Mathieson account for the machine hub-to-tip ratio rather than the aspect ratio.

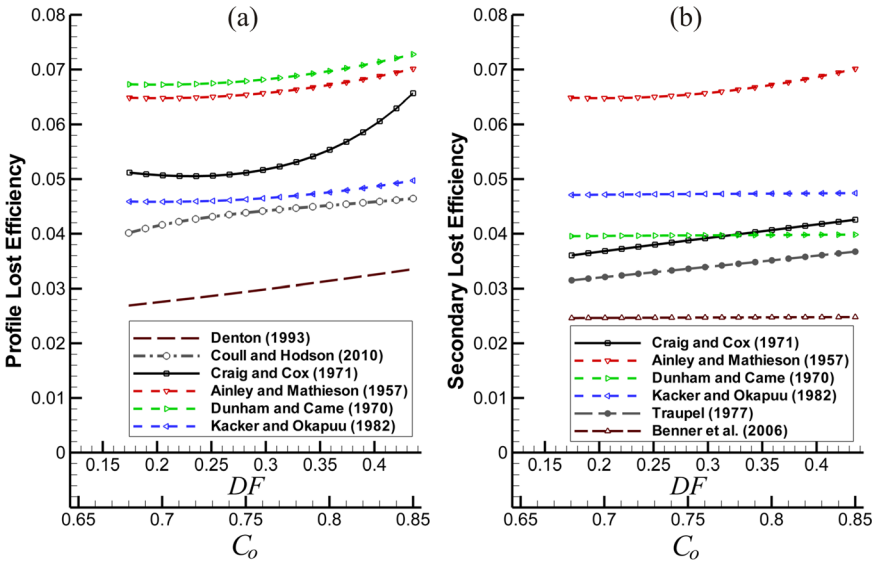

Fig. 12 Predicted lost efficiency with increasing lift for the datum flow angles ($\phi = 0.9$, $\psi = 2$).: (*a*) Profile Loss; (*b*) Secondary Loss

The reference velocity is therefore artificially low, and thus C_L is artificially high for such high-turning designs. Furthermore, Eq. (28) was formulated for relatively low turning blades and it is therefore of questionable validity. In comparison, Craig and Cox used results from a much wider range of blade designs to formulate their model.

Figure 11(*c*) shows the predictions according to Dunham and Came [3], who updated the Ainley and Mathieson secondary loss model to account for aspect ratio. Predictions using the subsequent modification by Kacker and Okapuu [9] are presented in Fig. 11(*d*). Both methods produce predict lower losses than the original method, which is arguably more realistic, but still predict the wrong efficiency trend across the design space.

Predictions using the correlation of Traupel [7] are presented in Fig. 11(*e*). This method successfully captures the loss of efficiency at high flow coefficient and low stage loading, and the predictions are very similar to those of Craig and Cox. (The very slight kinks at high stage loading coefficient are a result of extrapolating from Traupel's graphs.)

Figure 11(*f*) shows the predictions of the recent secondary loss correlation of Benner et al. [17], assuming that the displacement thickness of the inlet endwall boundary layer is $\delta^* = 0.05h$. This method correctly captures the increase in loss at high flow coefficients. Although promising, it is not clear how to select an appropriate value of δ^* at the preliminary stages of design, which has a large influence on the predictions.

Considering the trends across the design space, the secondary loss models of Craig and Cox and Traupel are the most reasonable of those considered. This analysis says nothing of the absolute accuracy of these correlations, which may only be determined by direct comparison of predictions and test data. It should also be noted that both methods are inherently approximate as they take no account of the shape of the surface velocity distributions, which are known to have a significant impact on the secondary losses. For example, Gier et al. [11] compared two high-lift LP turbine cascades with similar flow turning and loading. The velocity peak on the T162 design was relatively far forward on the surface, and this exhibited a 30% higher secondary loss coefficient than the aft loaded T161. The mean-line secondary loss models considered here lack the fidelity to capture this variation, and will therefore be prone to (significant) errors. There is therefore considerable scope to develop improved methods in the future.

5.3 The Influence of Blade Loading. In recent years a great deal of research has examined the performance of high-lift and ultra-high-lift blade designs for LP turbines. Higher lift designs require fewer blades and therefore offer a weight and cost saving for the engine, but tend to have lower efficiency. This section examines the trade-off between lift and efficiency.

Calculations are shown in Fig. 12 for designs with the same flow angles as the datum turbine ($\phi = 0.9$, $\psi = 2$) but varying lift. Figure 12(*a*) shows the lost efficiency due to profile loss alone. (Noting that these designs have velocity distributions of the style shown in Fig. 5, the diffusion factor for each design is also indicated on the horizontal axes.) The method of Denton [13] predicts the lowest loss, which is unsurprising since it assumes fully turbulent boundary layers. The Coull and Hodson [6] model indicates a modest increase in profile loss with increasing lift, consistent with such forward-loaded designs. However, there is a slight drop off in loss for designs with low lift ($DF < 0.20$), which is unlikely to be physical. Such designs are close to the limit of the high-lift experimental data used to formulate this method ([5]). It should also be noted that the Coull and Hodson method does not account for the base pressure loss on the turbine trailing edge, which can be significantly higher for lower lift designs. Figure 12 shows that the method of Craig and Cox [9] predicts a rapid rise in loss above $C_o \approx 0.77$, probably due to extrapolating beyond their experimental design space. The Ainley and Mathieson [3] and Dunham and Came [4] methods both predict very high profile losses. For this particular set of flow angles, the Kacker and Okapuu [5] correlation predicts similar values to the Coull and Hodson method.

The secondary lost efficiency is presented in Fig. 12(*b*) for the models considered in the previous section. Of these, the method of Ainley and Mathieson [3] predicts very high losses in line with Fig. 11. The models of Dunham and Came [3], Kacker and Okapuu [5] and Benner et al. [17] (assuming an inlet endwall boundary layer with $\delta^* = 0.05h$) predict that secondary loss stays almost constant with increasing lift. These predictions are contrary to experimental experience (e.g., Ref. [11]). The Craig and Cox [9] and Traupel [7] models predict a rise in secondary flow losses with lift, but the increase is significantly less than that observed by Gier et al. [11] and Praisner et al. [20] for high-lift LP turbine blades. Despite this inadequacy, these methods give the most realistic trends of the models considered.

5.4 The Influence of Reynolds Number. As an aircraft increases its altitude, the lower ambient pressure causes the blade Reynolds numbers to drop which reduces the efficiency of the low

pressure turbine. Since cruise performance is of crucial importance, it is desirable to predict this Reynolds number lapse at the preliminary design stage.

In the International Standard Atmosphere model, the variation of temperature with altitude is approximated by assuming that it decreases linearly with height:

$$T = T_{\text{sea}} - 0.0065 \times (\text{altitude in m}) \tag{31}$$

The pressure is then given by:

$$\frac{P}{P_{\text{sea}}} = \left(\frac{T}{T_{\text{sea}}}\right)^{5.256} \tag{32}$$

where P_{sea} and T_{sea} are the sea-level pressure and temperature, and the exponent (5.256) is related to the earth's gravitational field and the properties of air.

To examine the influence of Reynolds number, it is assumed that the nondimensional operating point of the turbine is constant, so that the same temperature and pressure ratios exist through the engine. The conditions at the inlet of the repeating turbine stage (P_{01}, T_{01}) at altitude are then governed by Eq. (32). Furthermore, for a given stage geometry the following nondimensional groups will remain constant:

$$\frac{\omega_s r_{\text{mean}}}{\sqrt{\gamma R T_{01}}}, \quad \frac{\dot{m}\sqrt{\gamma R T_{01}}}{(r_{\text{mean}})^2 P_{01}}, \quad \frac{\dot{w}_x}{(r_{\text{mean}})^2 P_{01}\sqrt{\gamma R T_{01}}}$$

These groups control the variation of dimensional shaft speed, mass flow rate and stage power as the stage inlet total pressure P_{01} and temperature T_{01} vary.

Calculations have been performed for the datum turbine operating at varying Reynolds number. Figure 13(*a*) shows the predicted lost efficiency due to profile loss alone. The influence of Reynolds number on each model may be summarized as follows: Denton [13] and Ainley and Mathieson [3] have no Reynolds number dependency; Dunham and Came [4] and Kacker and Okapuu [5] assume a turbulent trend ($\sim \text{Re}^{-0.2}$) for Reynolds numbers below 200,000; Craig and Cox [9] predict a turbulent trend across the whole Reynolds number range. In fact the measurements of Coull et al. [10] demonstrated that high-lift LP turbines of this style tend to exhibit a laminar trend ($\sim \text{Re}^{-0.5}$) at low Reynolds numbers and a turbulent trend ($\sim \text{Re}^{-0.2}$) at high Reynolds numbers, an effect which is captured in Fig. 13(*a*) by the Coull and Hodson [5] correlation. This method is therefore the most realistic.

The loss in efficiency due to secondary loss alone is presented in Fig. 13(*b*). Again, significant differences between the models are evident. The models based on Ainley and Mathieson ([2–4]) and the Benner et al. [17] correlation indicate no variation with Reynolds number. Craig and Cox [9] predict a turbulent trend across the whole Reynolds number range, while Traupel [7] assumes a laminar trend ($\sim \text{Re}^{-0.5}$) below $\text{Re}_C = 2 \times 10^5$. In reality, measurements of secondary losses generally show some increase in secondary losses at low Reynolds number (e.g., Refs. [21] and [22]) but there is no universally-observed trend. It is therefore unclear from this comparison whether the Reynolds number dependency of the Craig and Cox [9] and Traupel [7] methods are realistic.

To illustrate the influence of blade loading on the Reynolds number lapse, Fig. 14 shows the Reynolds dependency for designs with the datum flow angles ($\phi = 0.9$, $\psi = 2$) using the profile and secondary loss models of Coull and Hodson [6] and Traupel [7] respectively. A similar plot may be obtained using the Craig and Cox secondary model. The predicted efficiency when considering profile and secondary losses alone is presented together with the overall efficiency for four levels of lift. In line with experimental experience [10], the profile efficiency drops strongly at low Reynolds numbers particularly for the highest lift design. The secondary efficiency shows a similar trend but with a weaker dependency on Reynolds number.

5.5 Quantitative Predictions of Reynolds Number Lapse Rates. The analysis presented above focuses on the qualitative performance of the correlations, but it is also necessary to consider the absolute accuracy of the predictions. To this end, mean-line analysis has been performed for the 3-stage high-lift (HL) and ultra-high-lift (UHL) turbines examined by Haselbach et al. [8]. The two turbines had similar performance at sea level conditions, but the UHL design had a far more rapid drop-off in performance at lower Reynolds numbers. Table 2 compares the measured lapse rates to predictions using the profile method of Ref. [6] and the secondary loss models of Craig and Cox [9] and Traupel [7]. Both methods correctly predict a larger efficiency drop for the UHL design, but over-predict the lapse rates. The model of Traupel gives more realistic values than that of Craig and Cox.

The over-predicted lapse rates suggest that the Traupel and Craig and Cox methods are oversensitive to Reynolds number

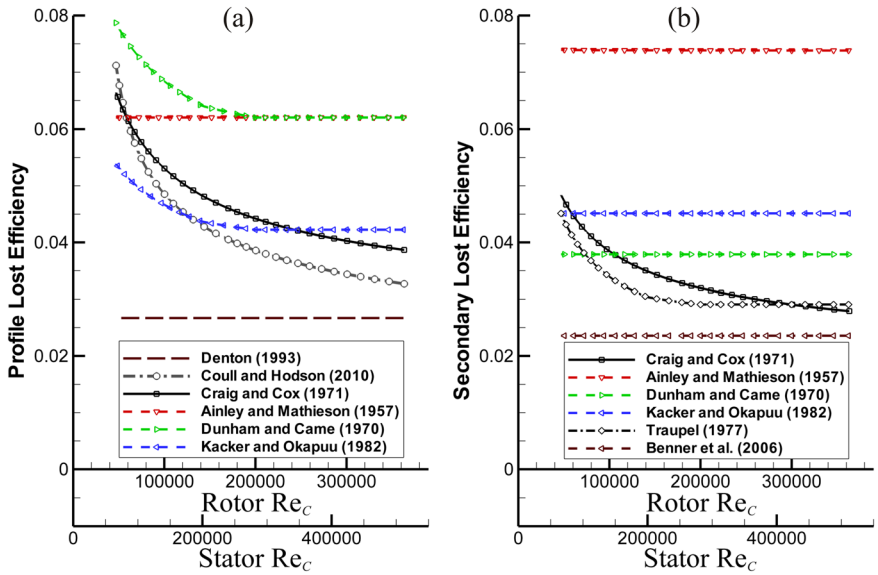

Fig. 13 Predicted lost efficiency with varying Reynolds number for the datum turbine: (*a*) profile loss; (*b*) secondary loss

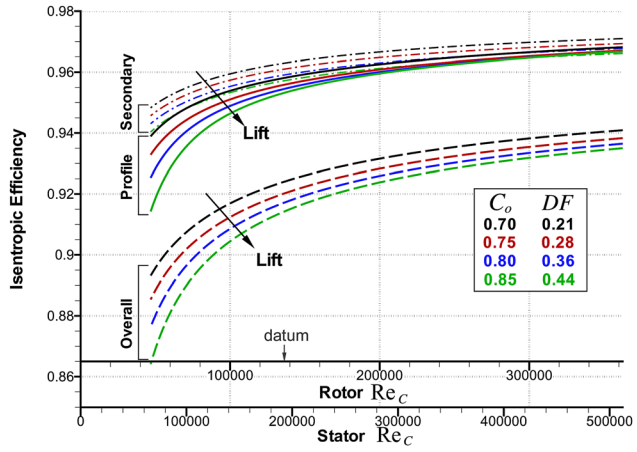

Fig. 14 Reynolds number lapse for varying lift, showing efficiency when considering profile loss alone [6], secondary loss alone [8] and the overall efficiency; datum flow angles ($\phi = 0.9$, $\psi = 2$)

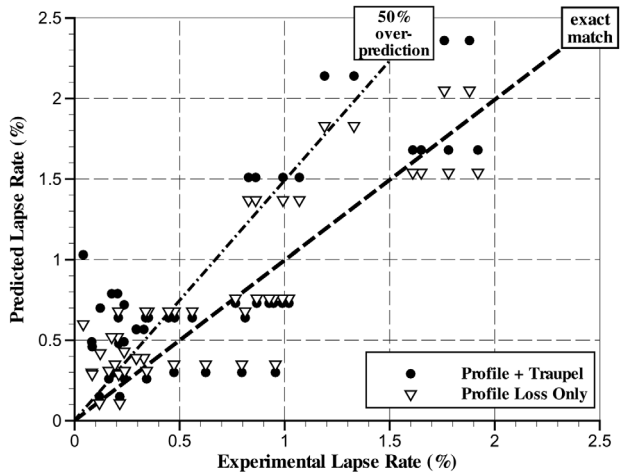

Fig. 15 Comparison of experimental and predicted efficiency lapse rates using the profile loss model of Coull and Hodson [6] Traupel [7] secondary loss model

variations. For example, in the recent rig measurements of Vázquez et al. [22] the secondary losses approximately followed a $\sim \mathrm{Re}^{-0.06}$ trend, which is significantly less sensitive than either of the Traupel or Craig and Cox models (Fig. 13(*b*)). Table 2 also shows the calculated loss of efficiency due to profile losses alone. These values are the lapse rates that would be predicted by a secondary model with no Reynolds number dependency (e.g., Refs. [2–4], and [17]). These profile-only predictions are closer to the experimental results but still over-predict the lapse rates. This is likely to be a consequence of the greater flow unsteadiness in the multistage environment compared to the experiments of Ref. [5]. Higher disturbance levels will tend to reduce separation bubble-induced losses at low Reynolds numbers, and increase losses at high Reynolds number by increasing the turbulent wetted area [10]. Both of these effects will tend to reduce the lapse rate.

Figure 15 shows a more extensive comparison between predicted and measured lapse rates for several multistage rig tests. The significant scatter on the plot is in part due to the spread of the experimental data. Predicted lapse rates have been calculated using the Traupel secondary loss model [7] and by considering profile losses alone [6]. In line with the results in Table 2, these methods tend to over-predict the lapse rates, on average, by around 30% and 15% respectively. This result reinforces the need to improve the understanding of secondary loss variation with Reynolds number, and the impact of the highly complex multistage environment on performance.

6 The Influence of Blade Loading on the Smith Chart Efficiency Contours

Finally, it is possible to estimate the influence of the lift coefficient on the efficiency contours of the Smith chart. Figure 16 shows efficiency contours for three circulation coefficients $C_o = 0.70,\ 0.75,\ 0.80$ (implying $DF = 0.21,\ 0.28,\ 0.36$) using the profile loss model of Coull and Hodson [6] and secondary model of Traupel [7]. (A similar chart may be obtained using the Craig and Cox secondary loss model.) As the lift is increased the contours retreat towards the bottom left of the chart, indicating that the efficiency decreases for a given set of flow angles. The retreat is not uniform, being far more gradual for the highly-turning blades towards the top left of the plot. These designs have low pitch-to-chord ratios and high exit angles, causing high profile losses. Equation (14) shows that profile loss tends to reduce with increasing pitch (due to a reduction in wetted area), which partly mitigates the increase in loss with lift.

Table 2 Predicted and measured Reynolds number lapse for the turbines examined by Haselbach et al. [9]

	Efficiency change, sea level to cruise	
Secondary Loss Model	HL	UHL
Craig & Cox	−2.35%	−2.52%
Traupel	−1.39%	−1.53%
Profile Losses Only	−1.29%	−1.45%
Experiments [9]	−0.9%	−1.3%

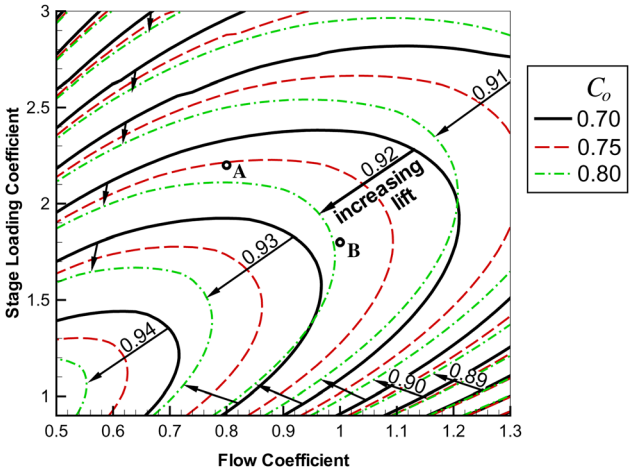

Fig. 16 Efficiency contours for three lift coefficients ($C_o = 0.70, 0.75\ 0.80$), using the profile loss model of Coull and Hodson [6] and secondary model of Traupel [7]

While the low sensitivity to lift is most apparent at the extreme top left of Fig. 16, the same trend is evident in the center of the design space. Two design points have been marked on Fig. 16 roughly indicate the practical limits of typical LP turbines flow angles: point A($\phi = 0.8$, $\psi = 2.2$) and point B($\phi = 1.0$, $\psi = 1.8$). Increasing the lift coefficient C_o from 0.70 to 0.80 causes an efficiency drop of 0.56% at point A, but a significantly larger drop of 0.86% at point B. Therefore the lower-turning design B is around 50% more sensitive to increases in lift than design A.

7 Conclusions

The Zweifel coefficient cannot meaningfully compare the lift of two blades with different flow angles. The root of the problem is the failure of Zweifel to account for blade curvature. An alternative lift coefficient based on circulation has been defined in an analogous fashion to the Zweifel coefficient. This Circulation Coefficient is directly related to the freestream velocity distributions over the blade surfaces, providing a meaningful measure of blade loading that is independent of the flow angles.

The loss correlations derived from Ainley and Mathieson [3–5] do not capture the correct trends for profile and secondary losses over the Smith chart design space and should therefore not be used for preliminary design. In particular the secondary loss models predict the *opposite* trend to that expected.

The profile loss model of Coull and Hodson [6] and the secondary models of Craig and Cox [9] and Traupel [7] produce realistic efficiency trends with respect to flow angles, lift coefficient and Reynolds number lapse rates, but tend to over-predict lapse rates. The Traupel secondary model gives more realistic quantitative predictions of lapse rates than the Craig and Cox method, but the Reynolds number dependency of both models needs to be revisited. The influence of the true multistage flow environment on performance also needs to be considered.

For typical LP turbine flow angles, designs with higher flow turning will tend to have lower sensitivity to increases in blade loading.

Acknowledgment

The authors would like to thank Dr. John Adamczyk and Professor John Denton for their comments on the analysis. Frank Haselbach and Julien Lefaivre of Rolls-Royce plc kindly provided the details for the turbine rig tests. Funding from EPSRC and Rolls-Royce is gratefully acknowledged.

Nomenclature

Symbols

b = camber-line length
C, C_x = true chord; axial chord
C_d = dissipation coefficient
C_o = circulation coefficient
DF = diffusion factor = $(U_{\text{peak}} - U_{TE})/U_{TE}$
f_r = S_0-based reduced frequency = $f_{\text{wake}} S_0/U_{TE}$
LEI = leading edge integral (Eq. (12))
Re_C = chord-based exit Reynolds number = $U_{TE} C/\nu$
Re_{S_0} = S_0-based exit Reynolds number = $U_{TE} S_0/\nu$
$\dot{m}$ = mass flow rate
P = pressure
r_{mean} = mean radius
s = pitch
S = surface distance from the leading edge
S_0 = suction surface length
t_{TE} = trailing edge thickness
T = temperature
U = blade velocity at mid-span
V_i, W_i = gas velocity in the absolute and relative frame
V_s = freestream velocity over blade surfaces
V_x, V_θ = axial and circumferential velocity components
$\dot{w}_x$ = stage power
Y = total pressure loss coefficient
Z_w = Zweifel lift coefficient
α_i, β_i = flow angles in the absolute and relative frame
δ^* = displacement thickness
ϕ = flow coefficient = V_x/U
η = isentropic stage efficiency
ν = kinematic viscosity
ρ = density
θ = momentum thickness
ω_s = shaft rotational speed
ψ = stage loading coefficient = $(\Delta V_\theta)_{\text{rotor}}/U$
ζ = total energy loss coefficient

Subscripts

0 = stagnation quantity
1 = stator inlet plane
2 = stator exit/rotor inlet plane
3 = rotor exit plane
is = isentropic
p = profile loss
peak = peak velocity on the suction surface
s = secondary loss
sea = sea level
TE = (suction surface) trailing edge

References

[1] Smith, SF., 1965, "A Simple Correlation of Turbine Efficiency," J. R., Aeronaut. Soc., **69**, pp. 367–370.
[2] Zweifel, O., 1945, "The Spacing of Turbomachine Blading, Especially with Large Angular Deflection" Brown Boveri Rev., 32(1), pp. 436–444.
[3] Ainley, D. G., and Mathieson, G. C. R., 1957, "A Method of Performance Estimation for Axial-Flow Turbines," ARC Reports and Memoranda Paper No. 2974.
[4] Dunham, J., and Came, P. M., 1970, "Improvements to the Ainley-Mathieson Method of Turbine Performance Prediction," Trans. ASME:, J. Eng. Gas Turbines Power, July, pp. 252–256.
[5] Kacker, S. C., and Okapuu, U., 1982, "A Mean Line Performance Method for Axial Flow Turbine Efficiency," J. Eng. Power, **104**, pp. 111–119.
[6] Coull, J. D., and Hodson, H. P., 2011, "Predicting the Profile Loss of High-Lift Low Pressure Turbines," J. Turbomach., **134**(2), pp. 021002-1– 021002-14.
[7] Traupel, W, 1977, *Thermische Turbomaschinen*, Springer-Verlag, Berlin.
[8] Haselbach, F., Schiffer, H. P., Horsman, M., Dressen, S., Harvey, N., and Read, S., 2002, "The Application of Ultra High Lift Blading in the BR715 LP Turbine," ASME J. Turbomach. **124**(1), pp. 45–51.
[9] Craig, H. R. M., and Cox, H. J. A., 1971, "Performance Estimation of Axial Flow Turbines," Proc. Inst. Mech. Eng., **71**, pp. 1970–1971.
[10] Coull, J. D., Thomas, R. L., and Hodson, H. P., 2010, "Velocity Distributions for Low Pressure Turbines," J. Turbomach., **132**(4), pp. 041006-1–041006-13.
[11] Gier, J., Franke, M., Hübner, N., and Schröder, T, 2008, "Designing LP Turbines for Optimized Airfoil Lift," ASME Paper No. GT2008-51101.
[12] Horlock, J. H., 1966, "Axial Flow Turbines: Fluid Mechanics and Thermodynamics," SBN 0-88275-097-6.
[13] Denton, JD, 1993, "Loss Mechanisms in Turbomachines" ASME J. Turbomach., **115**(4), p. 621–656.
[14] Ainley, D. G., and Mathieson, G. C. R., 1951, "An Examination of the Flow and Pressure Losses in Blade Rows of Axial-Flow Turbines," ARC Reports and Memoranda Paper No. 2891.
[15] Carter, ADS, 1948, "Three-Dimensional Flow Theories for Axial Compressors and Turbines," Proc. Inst. Mech. Eng., **159**(1), pp. 255–268.
[16] Thwaites, B., 1949, "Approximate Calculation of the Laminar Boundary Layer," Aeronaut. Q., **1**, pp. 245–280.
[17] Benner, M. W., Sjolander, S. A., and Moustapha, S. H., 2006, "An Empirical Prediction Method For Secondary Losses In Turbines – Part II: A New Secondary Loss Correlation," J. Turbomach., **128**(2), pp. 281–291.
[18] Vera, M., Hodson, H. P., and Vazquez, R., 2003, "The Effect of Mach Number on LP Turbine Wake-Blade Interaction" 9th ISUAAAT, Sept. 4–8, Lyon, France
[19] Marconcini, M., Rubechini, F., Pacciani, R., Arnone, A., and Bertini, F., 2010, "Redesign of High-Lift LP-Turbine Airfoils For Low Speed Testing" ASME Turbo Expo, Glasgow, UK, 14–18 June, ASME Paper No. GT2010-23284.
[20] Praisner, T. J., Grover, E. A., Knezevici, D. C., Popovic, I., Sjolander, S. A., Clarke, J. P., and Sondergaard, R., 2008, "Towards the Expansion of Low-Pressure-Turbine Airfoil Design Space," ASME Paper No. GT2008-50898.
[21] Hodson, H. P., and Dominy, R. G., 1987, "The Off-Design Performance of a Low-Pressure Turbine Cascade" ASME J. Turbomach. **109**(2), pp. 201–209.
[22] Vázquez, R., Torre, D., Partida, F., Armañanzas, L., and Antoranz, A., 2011, "Influence of Surface Roughness on the Profile and End-Wall Losses in Low Pressure Turbines," ASME Paper No. GT2011-46371.